On the combination of ultraviolet photoelectron spectroscopy with optical absorption studies to investigate $Cu_2O||TiO_2$ direct Z-scheme junctions with different Cu_2O loading

Reference:

de la Fuente Beatriz, Bomnüter Jan, Del Moro Michele, Smeesters Lien, Cristaudo Vanina, Breugelmans Tom, Meynen Vera, Cool Pegie, Hubin Annick, Hauffman Tom.- On the combination of ultraviolet photoelectron spectroscopy with optical absorption studies to investigate $Cu_2O||TiO_2$ direct Z-scheme junctions with different Cu_2O loading
Applied surface science - ISSN 1873-5584 - 657(2024), 159796
Full text (Publisher's DOI): https://doi.org/10.1016/J.APSUSC.2024.159796
To cite this reference: https://hdl.handle.net/10067/2047040151162165141

On the combination of ultraviolet photoelectron spectroscopy with optical absorption studies to investigate $Cu_2O||TiO_2$ direct Z-scheme junctions with different Cu_2O loading

Beatriz de la Fuente[1*], Jan Bomnuter[2], Michele del Moro[3], Lien Smeesters[4], Vanina Cristaudo[1], Tom Breugelmans[3], Vera Meynen[2], Pegie Cool[2], Annick Hubin[1], Tom Hauffman[1]

[1] *Research Group Electrochemical and Surface Engineering SURF, Department Materials and Chemistry, Vrije Universiteit Brussel, Pleinlaan 2, 1050 Brussels, Belgium*

[2] *Laboratory of Adsorption and Catalysis LADCA, University of Antwerp, Universiteitsplein 1, 2610 Antwerpen, Belgium*

[3] *Applied Electrochemistry and Catalysis ELCAT, University of Antwerp, Universiteitsplein 1, 2610 Antwerpen, Belgium*

[4] *Brussels Photonics B-PHOT, Department of Applied Physics and Photonics, Vrije Universiteit Brussel, Pleinlaan 2, 1050 Brussels, Belgium*

Correspondence should be addressed to B. de la Fuente (email: Beatriz.de.la.fuente.perez@vub.be)

KEYWORDS

Titania nanotubes
Work function
Ionization potential
Ultraviolet Photoelectron Spectroscopy (UPS)
Z-scheme

ABSTRACT

Among the electronic properties, the positions of the electronic band edges and the work function are essential parameters for determining the potential of a photocatalyst and its ability to function in a solar conversion system. A novel type of photocatalysts, called direct Z-schemes, possesses many advantages over conventional heterojunctions, which all benefit the catalytic performance under solar light. As oxidation and reduction reactions are greatly affected by the electrical characteristics of the material, ultraviolet photoelectron spectroscopy (UPS) is a powerful tool to determine and quantify important electronic parameters of previously fabricated $TiO_2||Cu_2O$ junctions. TiO_2 nanotubes modified with Cu_2O nanoparticles exhibit a reduction in the value of the work function (WF = 3.67 ± 0.01 eV) and ionization potential (IP = 6.01 ± 0.04 eV) with respect to the TiO_2 substrate (WF = 4.29 ± 0.02 eV and IP = 7.65 ± 0.05 eV). By varying the electrodeposition time, an optimized amount of deposited Cu_2O nanoparticles was proven to reduce the WF and IP to facilitate the excitation of electrons, which could be correlated to the improved absorbance in the visible wavelength range. This work proposes a valuable methodology for band diagram tracing from UPS spectra and provides new insights in the relationship between synthesis, electronic properties and visible light absorption of titania based Z-schemes for photocatalytic applications with a combination of surface sensitive techniques and optical absorption studies.

1. Introduction

Driven by climate change alongside geo-environmental and -economic considerations, more and more efforts are devoted towards the development of new active materials for the photo(electro)catalytic conversion of CO_2 with H_2O into essential feedstocks and fuels [1]–[3]. Increasing importance is given to designing efficient semiconductor photocatalysts to provide a carbon-neutral, renewable, and scalable energy source because of their ability of using the energy from the sun to induce various photocatalytic reactions [4]. Similar to what happens during natural photosynthesis, the energy of sunlight is used to convert H_2O and CO_2 into O_2 and recoverable hydrocarbons at the surface of a light-active material [5].

The first photocatalytic conversion of CO_2 was reported in 1979. The final products obtained from CO_2 reduction were several organic compounds such as methane and its intermediates by Xenon lamp radiation in the presence of light sensitive catalytic powders [6]. Many following studies have used a wide range of different semiconductors to reduce CO_2 into hydrocarbons using visible light, ranging from metal chalcogenides [7], metal oxides including TiO_2[8]–[10], Fe_2O_3[11], Cu_2O[12], [13] and perovskite metal oxides such as $BiVO_4$[14] and WO_3[15], [16]. These all have all been identified as potential candidates to work under solar light.

A new type of photocatalytic systems made out of two or more semiconductors are the so-called *direct Z-schemes.* Imitating what occurs during natural photosynthesis in plants, these systems possess many advantages over conventional junctions. Figure 1 shows the typical electrons and holes transfer in a Z-scheme junction. Upon light irradiation on the surface, electron/hole pairs are generated. The generated electrons with higher reduction power in the conduction band (CB) of photosystem II and holes with higher oxidation power in the valence band (VB) of photosystem I are preserved, while the generated electrons with lower reduction power in the CB of photosystem I and holes with lower oxidation power in the VB of photosystem II recombine. Recent studies have pointed out the several advantages of building direct Z-scheme photocatalysts to drive an efficient CO_2 reduction reaction via solar energy [17]–[20]. These include the removal of ineffective photogenerated pairs with weaker redox power, the preservation of beneficial photogenerated pairs with higher redox power and the efficient locally separated active sites, which all benefit the catalytic performance of the fabricated material [17].

Given its capacity to break down organic contaminants and its corrosion resistance, durability, abundance, and affordability, TiO_2 is one of the most often used catalysts [21]. With its band positions that are ideal for CO_2 conversion and water splitting, it is considered a promising material and is widely utilized both as a catalyst for photo-electrocatalytic processes [22], [23] and as an electrode material in photovoltaics [24], [25]. TiO_2 nanotube (NT) arrays provide a number of advantages over other microscopic morphologies. They can improve electron transport efficiency and prevent charge carrier recombination thanks to their distinctive tube-shaped structure [26]. Moreover, this type of microstructure has a much better recyclability compared to TiO_2 powders [27]. TiO_2 NT also have a surface area of >30m^2/g and high surface energy (> 70 mJ/m^2), essential characteristics for a catalyst that are positively related to higher catalytic activity [28], [29]. Combining it with cuprous oxide Cu_2O, which presents wide availability, low cost, and a high light absorption coefficient ($\alpha \sim 104$ cm^{-1}) in the 380-700 nm region, has been demonstrated to be an efficient technique to design an optimal direct Z-scheme [17]. By creating and characterizing a heterostructure made of octahedral Cu_2O and TiO_2 nanoparticles, Aguirre et al. directly demonstrated the effectiveness of the Z-scheme in the reduction of CO_2 [30]. However, information about the optimization of the deposition time of the Cu_2O phase needed to reach optimal absorption in the UV and visible light range is still missing.

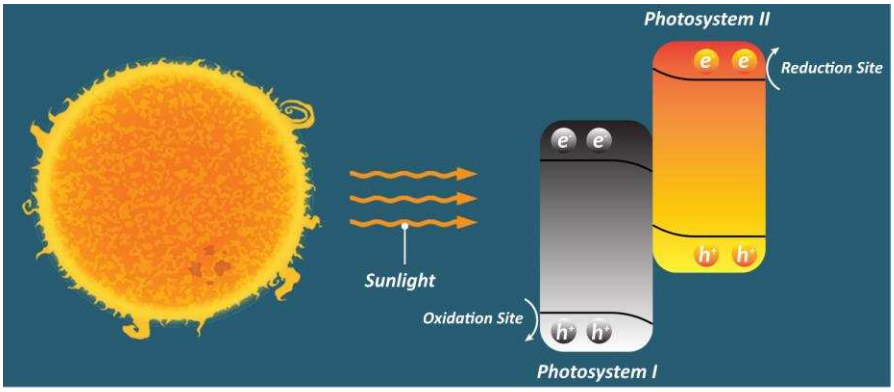

Figure 1: Schematic working mechanism of direct Z-schemes.

To maximize the separation efficiency between electrons and holes and tune the selectivity of the photocatalytic reaction toward various desired products, it is crucial to have a thorough grasp of the functioning mechanism of Z-scheme photocatalysts [18]. This is done by using nanoscaled molecular surface characterization techniques that allow to extract the electronic properties of the photocatalyst. Knowledge of their electronic structure is of importance because it dictates their efficiency in solar conversion systems. The electronic structure is made of parameters such as the Fermi energy level (E_F), work function (WF), energy band gap (E_G), ionization energy (IP), and electron affinity (EA). Furthermore, the level offset between the VB and CB of the materials forming a heterojunction determines whether charge transfer will be facilitated or hindered [31]. The measurement of the WF is of special importance when designing materials for photocatalysis as it governs the band alignments of interfaces such as TiO_2/metal and TiO_2/metal oxide contacts [32]. The WF gives an indication of the energy required to bring an electron from deep inside the material to a point just outside the surface. It thus directly depends on the position of the vacuum and Fermi levels [33].

Ultraviolet Photoelectron Spectroscopy (UPS) presents itself as a potential tool to determine the WF of electronic and functional materials, the IP, and EA (the latest with an additional low energy inverse photoemission measurement). Other techniques exist to study the electronic parameters of these materials, such as thermionic emission (TE), field emission (FE), and the Kelvin probe technique (KP). However, TE requires samples with high-temperature endurance (2500°C, well above the limit at which TiO_2 structural and chemical properties become altered), FE presents disadvantages such as space-charge effects that can happen on the tip radius and microfield, limiting the further emission of electrons from the surface, and the KP does not give the WF in an absolute manner but rather in a relative one with respect to another material. It thus requires a reference electrode material, usually gold [34]–[37]. UPS, based on photoelectric emission (PE), uses a helium discharge lamp that produces light with a wavelength of 58.4 nm (21.2 eV) in the vacuum ultraviolet region and then measures the kinetic energies of photoelectrons ejected that reach its electron analyzer. This technique allows an accurate determination of the secondary electron cut-off for the absolute WF and IP obtention [38], [39].

This work is the first application of UPS to study the relationship between Cu_2O electrodeposition time and electronic properties of $Cu_2O||TiO_2$ direct Z-scheme materials. The novelty of this work concerns the several insights that can be derived from UPS on previously fabricated TiO_2/Cu_2O heterojunctions and underlines which important electronic parameters can be extracted from the spectra to help with the band diagrams tracing task. Furthermore, a laboratory scale investigation is implemented to evaluate the visible light absorption performance of $Cu_2O||TiO_2$ under various electrodeposition conditions. Therefore, this novel approach, combining UPS and optical spectroscopy, allows to correlate synthesis (electrodeposition time), electronic properties, and absorption profiles.

2. Experimental

2.1 Anodization

The Ti-felt (NV Bekaert SA, 1.0 x 3.0 cm²) was placed overnight in a beaker with acetone (Fisher Scientific, ≥ 99.8%) on a stirring plate. Then, the felt was washed with distilled water and dried with compressed air. Subsequently, the Ti-felt was anodized with a power supply unit (TENMA bench power supply) at static conditions and at room temperature in the electrolyte containing 94.5 wt.% ethylene glycol (Supelco, ≥ 99%), 5.0 wt% distilled water and 0.5 wt% ammonium fluoride (Alfa Aesar, ≥ 98%) with a Pt gauze as the cathode, applying a potential of 25 V for one hour in order to form nanotubes [40]. Afterwards, the felt was rinsed thoroughly with distilled water and calcined at 450 °C (5°C/min) in air for two hours.

2.2 Electrodeposition of Cu_2O

Even though we acknowledge that a full parameter-to-electronic properties screening and characterization would be an intriguing path to follow for further studies, this work focuses on the effect of deposition time based on an established peer-reviewed procedure. Therefore, the Cu_2O nanoparticles were electrodeposited adapting the procedure reported by Li et al [41]. The deposition was carried out using a potentiostat (Autolab PGSTAT302F), in a three-electrode set-up with the TiO_2-felt as working electrode, a Pt gauze as counter electrode, and a Ag/AgCl (Sat. KCl) electrode as reference electrode. The electrolyte consisted of 0.4 M copper(II)sulfate (VWR, ≥ 99%) and 3.0 M lactic acid solution (Sigma-Aldrich, 85 wt.%), whereby the pH was adjusted slowly to 11 with sodium hydroxide pellets (Acros Organics, ≥ 98.5%). The temperature was adjusted to 60 °C. In Li's article, the electrodeposition was performed at -12 mA/cm², however, in our case, this would result in non-homogeneous layers. Thereby, a current density of -4 mA/cm² was applied to the TiO_2 NT felt under static conditions. Three samples, *S15*, *S30*, and *S45*, were prepared using electrodeposition times of 15, 30, and 45 minutes, respectively. 15 minutes was selected as the minimum deposition time due to synthesis restrictions. Immersion in a 10 vol.% ammonia solution (Thermo Scientific, 28-30 wt.%, analysis grade) for 10 min was done to remove residual Cu^{2+} ions from the surface. This was followed by a step of thorough rinsing with H_2O and of drying overnight at 40 °C. A pure TiO_2 felt sample was kept as a control, further referred to as *substrate*. The samples were kept under ambient air condition.

2.3 Surface characterization

Morphologies were investigated with a high-resolution JEOL JSM-7100F field emission scanning electron microscope (FE-SEM) under 15kV acceleration voltage. This instrument was equipped with an Oxford Instrument X-MaxN Silicon Drift Detector for Energy-Dispersive X-ray Spectroscopy that was used to study the phase distribution of the deposited Cu_2O phase.

The chemistry and oxidation states of the samples were studied using a VersaProbe III X-ray photoelectron spectroscope (XPS) operating with an Al Kα anode and a main chamber pressure of 5×10^{-7} Pa. High-resolution scans of the C1s, O1s, Ti2p, Cu2p photoelectron peaks, and Cu LMM Auger peaks were recorded with an angle of 45° regarding the sample normal. The selected pass energy was 280 eV and 26 eV and the step size 1 eV and 0.1 eV for the surveys and high resolution scans, respectively. Three different spots per sample were recorded. Data quantification and curve fitting were done with CasaXPS software (version 2.3.24PR1.0). The sensitivity factors used were taken from the MultiPak Software manual (v. 9) and were used to compute the atomic concentrations of each element. The C1s photoelectron peak was divided into the following components, all of which had the same full width at half maximum (FWHM) value: C-C/C-H, C-OH/C-O-C, C=O, and O-C=O. The line shape of the different components used was a Gaussian – Lorentzian line shape (GL(30)). Calibration of the binding energy (BE) scale of every sample was done by associating the C-C/C-H component from the C1s high resolution spectra to its respective BE at 284.8 eV.

X-ray diffraction (XRD) was applied to characterize the crystal phases of the samples. The measurements were performed by a D8 advance Eco diffractometer with Cu-Kα radiation (λ= 1.5406 Å) at a scanning range of 10–80° 2θ and a scanning rate of 0.04°/4 s. The XRD patterns of all the samples were normalized by dividing every peak by the most intense peak to get relative intensities.

Ultraviolet photoelectron spectroscopy (UPS) was also performed using the VersaProbe III spectroscope with a He I (21.2 eV) light source (wavelength of 58.4 nm). To ensure proper electrical contact, the samples were mounted using copper tape and a metallic shield provided by the manufacturer, as shown in the procedure from Figure S1. The holder used was a 25 mm one, allowing the sample tilting that is required for UPS.

The samples were then presputter-cleaned with a GCIB gun (10kV, 30nA, 5x5mm). A negative potential of -5V was provided to the samples to reduce surface charging and to separate the secondary edges of the sample and analyzer. The sputter-cleaned Ag sample was used to calibrate the binding energies attained for UPS. All values determined from UPS analysis are related to the vacuum. The determination of the electron cut-off (E_{cutoff}), valence band maximum (E_{VBM}), and Fermi level (E_F) was conducted with the Edge tool from the PHI MultiPak software. The E_{cutoff} and E_{VBM} values were extracted by using Multipak's edge tool that linearly fits the spectrum and intercepts the x-axis with the created fit. From these parameters, the WF and IP values were calculated. The WF and IP of all samples were computed using the Edge tool function from the Multipak software and the formulas below.

$$WF = hv - (E_{cutoff} - E_F) \qquad [1]$$

$$IP = hv - (E_{cutoff} - E_{VBM}) \qquad [2]$$

Two different batches were tested with the same synthesis conditions to ensure reproducibility and three points were examined for each sample prepared. The calculated error was included as standard deviation.

2.4 Optical absorption studies

The visible absorption spectrum was determined by measuring the transmitted and reflected light and considering that the sum of the light absorbance, transmittance, and reflectance equals 100% of the light according to the conservation of energy. Measurements were performed using a pigtailed halogen light source (335 – 2500 nm), enabling the broadband spectral illumination of the sample. Both transmission and reflection measurements were performed using an irradiance and reflection integrating sphere (Avants AvaSphere-30-irrad and AvaSphere-30-refl), respectively, enabling the collection of all transmitted and reflected light independent of the emission angle. During the transmission measurements, the source fiber was positioned perpendicular to the sample surface, while an illumination angle of 8° was present during the reflection measurements. Both integrating spheres were coated with a reflective Spectralon® coating (> 98 % reflectance), ensuring that the collected light is guided towards the detection port. The collected light is subsequently guided to the optical spectrometer (Avantes AvaSpec3684) using a multimode optical fiber (Avantes FC-UVIR600-2). The spectrum is measured from the ultraviolet to near-infrared wavelength range, starting from 350 nm until 1100 nm, featuring a spectral resolution of 1.4 nm. An absolute reflectance measurement was performed, taking into account the spectral characteristics of the source and the background light, by measuring the reference and dark spectrum, respectively. The reference spectrum is a measure of the source spectrum, corresponding to the transmission measurement in absence of a sample, and to the reflection measurement of a calibrated 99.9% diffuse reflectance standard (Spectralon® SRS-99-10). The measurements were performed in a controlled laboratory environment, without the presence of background lighting, maximizing the dynamic range. The spectra are recorded using the Avantes Avasoft 8 software package and subsequently processed using Matlab.

3. Results and discussion

3.1 Surface morphology with FE-SEM

The morphology of the *substrate* sample was investigated with FE-SEM, to confirm the presence of properly aligned TiO_2 NT were present before the electrodeposition of Cu_2O. The nanotubes must be well aligned to facilitate charge transfer and future optimal activity under light irradiation. Figure 2 (A) shows the TiO_2 layer formed on the Ti felt by anodic oxidation. The average NT diameter was of 55.8 ± 3.6 nm. On samples that had been mechanically bent, cross-sectional measurements were made to estimate the length of the nanotubes (~1080 nm). The mean value of the length was based on three measurement points, as shown in Figure S2. The anodization step was followed by an electrodeposition step to decorate the TiO_2 NT with Cu_2O nanoparticles. Figure 2 (B), (C), and (D) show FE-SEM topographical images of the TiO_2 NT substrate after modification with Cu_2O under 15, 30, and 45 minutes, respectively. A deposition time of 15 minutes led to homogeneously distributed Cu_2O NP with an average particle size of 0.16 ± 0.04 µm, based on 12 measurement points, shown in Figure 2 (B). Longer deposition times (30 minutes) led to an increased average particle size of 0.40 ± 0.11 µm, also based on 12 measurement points, and in an increased surface coverage, shown in Figure 2 (C). Increasing the time to 45 minutes led to the entire TNT surface being covered with a Cu_2O phase which obstructed the TiO_2 tube openings, shown in Figure 2 (D). This obstruction was not observed in the case of 15 and 30 minutes electrodeposition time, despite the size of the Cu_2O particles being much larger than the TiO_2 NT in all three cases. Additionally, it has been previously reported that smaller particle sizes (<100nm) benefit charge transfer [42], [43]. The condition under 15 minutes yields particle sizes that approximate that reported value the most.

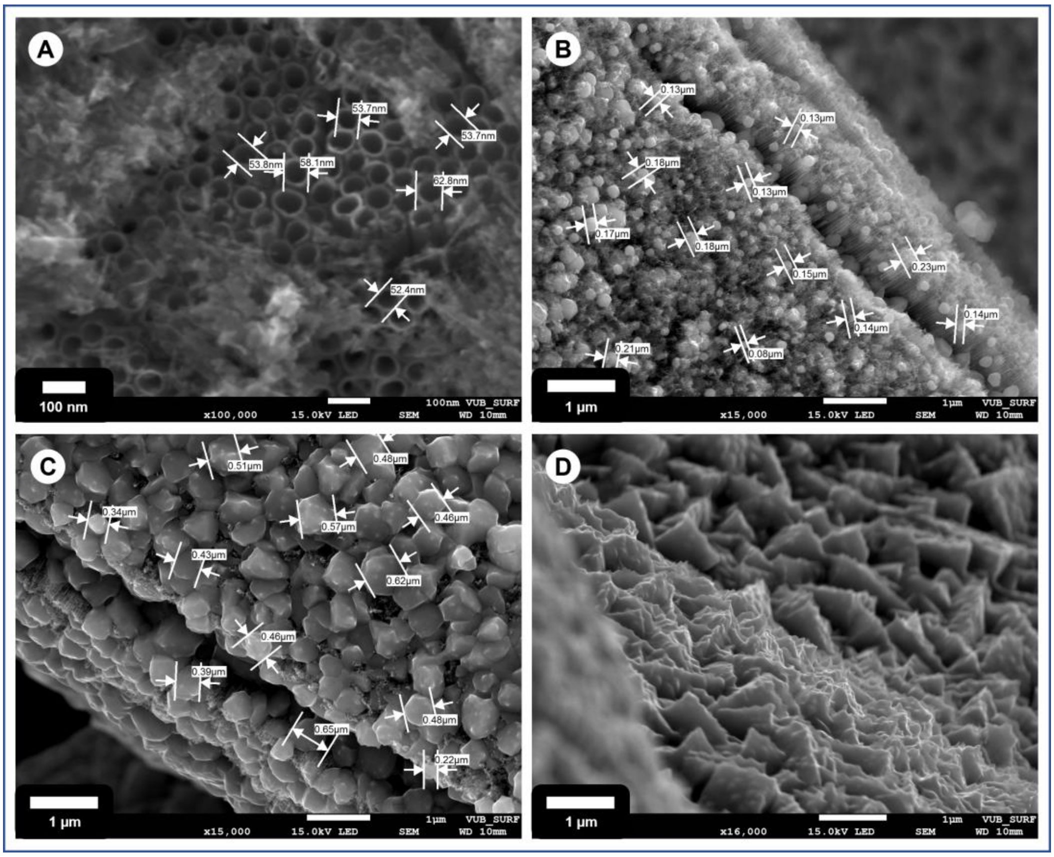

Figure 2: FE-SEM images of (A) the TiO_2 substrate and the Z-schemes under (B) the 15 minutes, (C) the 30 minutes, and (D) the 45 minutes electrodeposition condition with their respective magnification.

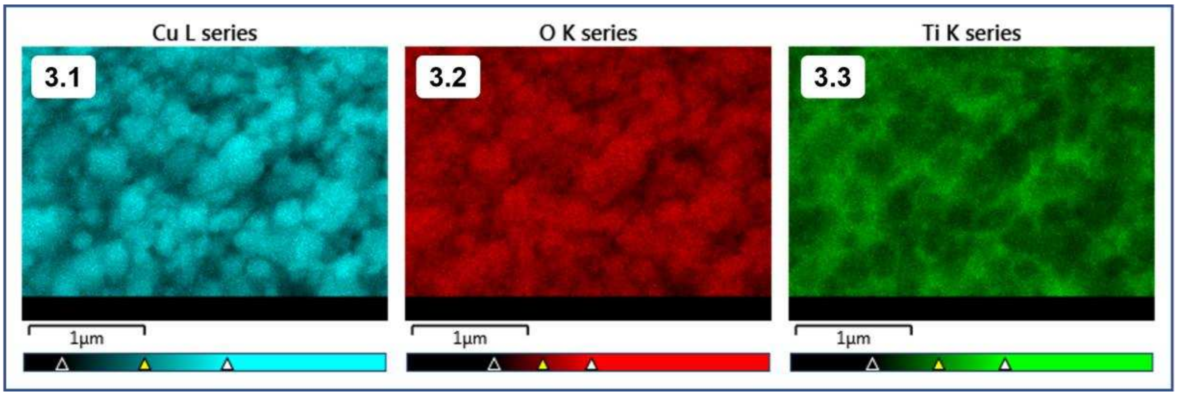

Figure 3: EDX mapping of the Z-scheme under 15 minutes of electrodeposition condition.

EDX was used complementarily to FE-SEM to analyze the elements present at the surface and to provide insights into the deposition surface distribution via specimen mapping. Figure 3 reports the Cu, O, and Ti specimen maps of S15 and shows that the deposited nanoparticles are enriched in Cu and O, as desired. The distribution of the copper oxide phase is observed at surface level, with the diameter of the nanotubes being of smaller size than the Cu_2O particles. Previous studies such as one from Macak et al. show the procedure of filling TiO_2 nanotubes by Cu_2O electrodeposition and indicate a possible minor contribution of Cu_2O nanoparticles deposited inside the nanotubes due to confinement effects [44]. However, the horizontal cross-sections of the NT do not show a filling and the major contribution reported is the superficial one. The steps followed from the growth of the titania NT substrate to the obtention of the Z-schemes, with varying surface coverage depending on the reduction time of the copper phase are shown on Figure 4. It should be noted that the schematic representation is not real to size, the Cu_2O particles size has been reduced for visual simplicity.

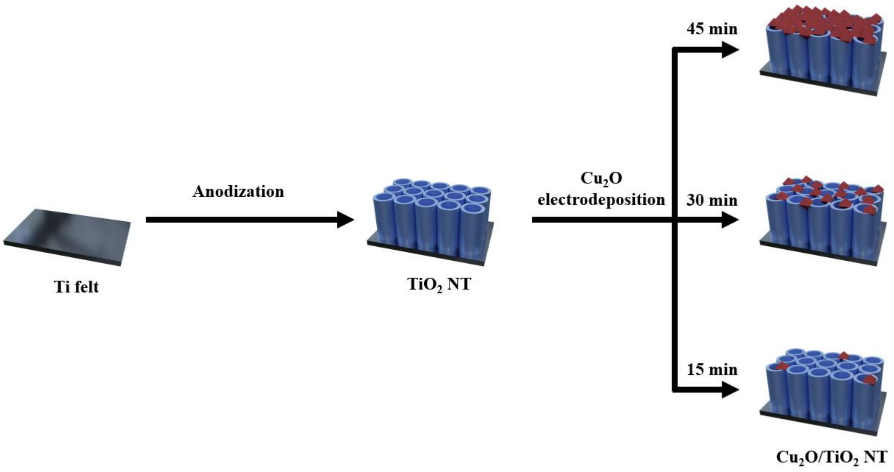

Figure 4: Schematic representation of the copper deposition using different deposition times. Representation not real to size for visual simplicity.

3.2 Surface chemistry, oxidation states and structure

XPS allowed to study the chemistry and elemental states present at the surface and thus validate the correct synthesis of the substrate and Z-schemes. Quantitative analysis was done with XPS and the CasaXPS software. Figure 5 shows the survey scan recorded, and Table 1 reports the atomic percentages of every element present in the sample. As expected, the atomic percentage of copper increases with increasing electrodeposition times. The standard deviations were located in the range of ± [0.80 ; 1.04] at%. These results further confirm, in a quantitative manner, the previously shown FE-SEM results. With increasing deposition times, the Cu is increasingly covering the titania so the thicker the layer deposited, the lower the Ti at% that is detected with surface sensitive XPS.

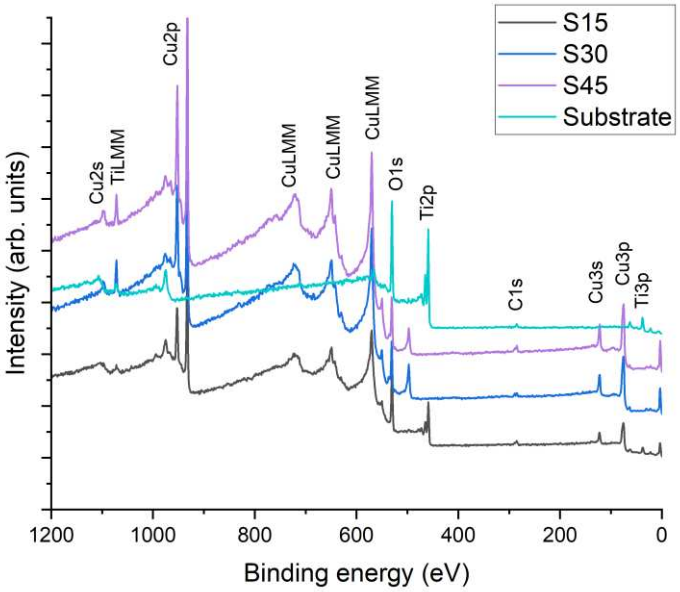

Figure 5: XPS survey scan of the substrate, S15, S30, and S45, on which the quantification is based.

Table 1: Elemental composition quantification: percentage atomic concentrations of the different elements in each sample with standard deviations located in the range of ±[0.80;1.04] %at.

Sample	*O1s*	*C1s*	*Ti2p*	*Cu2p*
Substrate	62.3	10.6	27.1	0
S15	62.2	6.8	22.5	8.5
S30	59.2	7.1	18.9	14.8
S45	54.0	9.2	6.2	30.6

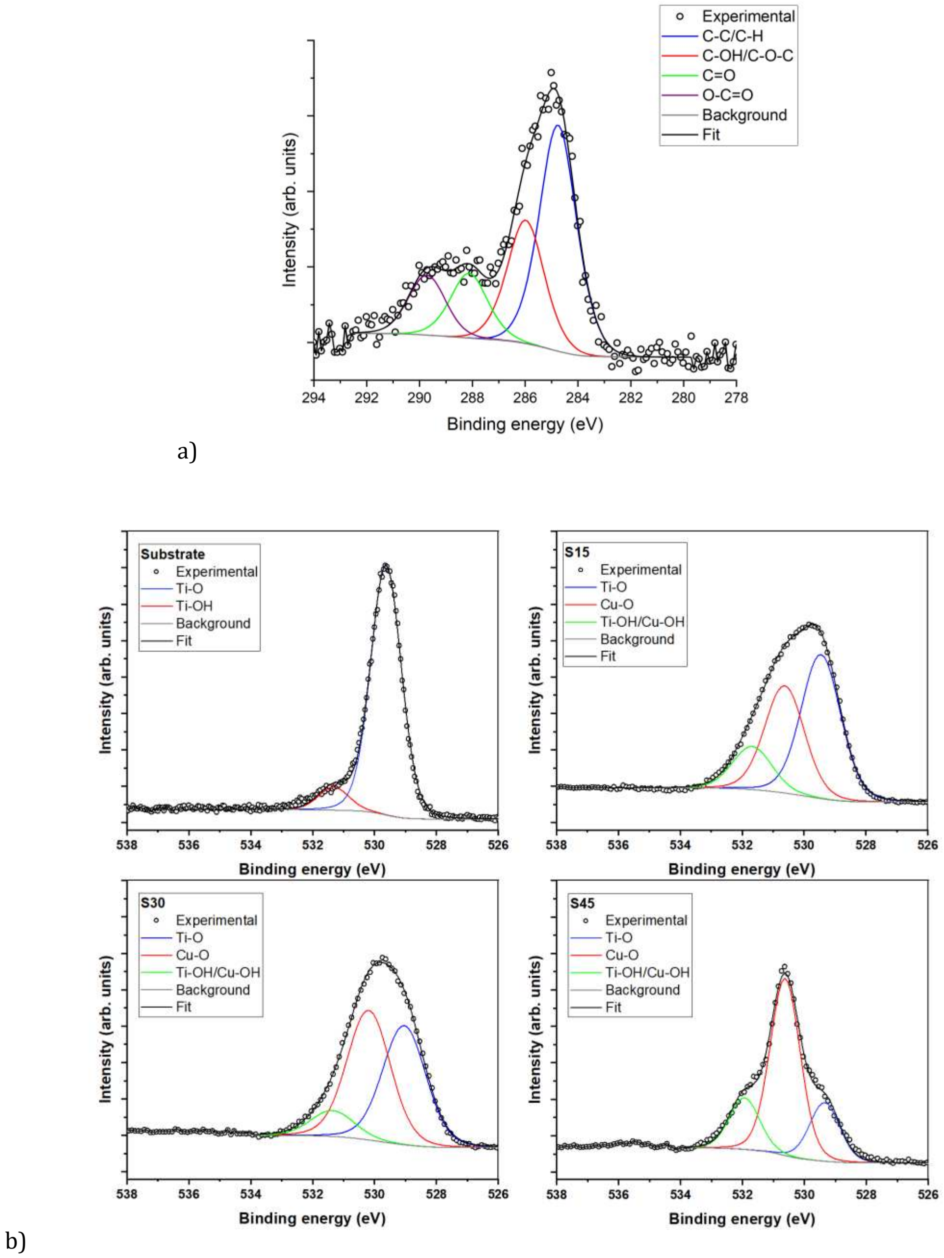

Figure 6: (a) C1s high-resolution spectra of S15, peak fitted [45] *and (b) O1s high-resolution spectra of the substrate, S15, S30, and S45, fitted and compared.*

The C1s and O1s photoelectron peaks were studied and are shown in Figure 6. The constraints put on the FWHM and the starting positions of the binding energies were the same as the ones reported previously in a work that reported the use of unintended carbon deposition at the surface for charge referencing purposes [46]. In Figure 6 (b), representative high resolution O1s spectra from the sputter cleaned substrate and Z-schemes are shown to see the tendencies of the compositions in the different samples. For the substrate, two contributions can be observed, namely Ti-O from TiO_2 in blue and Ti-OH in red. For the electrodeposited samples, three contributions can be observed. The component in blue was assigned to Ti-O from TiO_2, this component typically being located at 529.4 eV; the component in red was assigned to the O in a Cu_2O lattice which is typically located at 530.5 eV [47]; and the component in green with the highest BE was assigned to hydroxyl Ti-OH/Cu-OH groups typically located at 531.3 and 531.2 eV, respectively [8], [9]. Hydroxyl groups may form at the surface when the samples become exposed to the atmosphere during storage and transfer. Additionally, a small amount of organic oxygen will also be present in the unintendedly deposited carbon overlayer. Some carbon residues can as well be present at the surface as a result of calcination of some small amount of organic compound originating from the electrolyte used for anodization. This organic oxygen peak is typically located at 531.0 eV [48]. The three aformentioned contributions had the same FWHM as a fixed condition, with a value of 1.42 eV. All the associated binding energies are shown in Table 2.

Table 2: Binding energies (eV) of the components used in the fitting of the O1s peaks. Standard deviations are located in the range of ±[0.03;0.14] eV.

Sample	*Ti-OH/Cu-OH*	*Cu-O*	*Ti-O*
substrate	531.6	-	529.6
S15	531.5	530.6	529.4
S30	531.3	530.4	529.2
S45	531.5	530.6	529.4

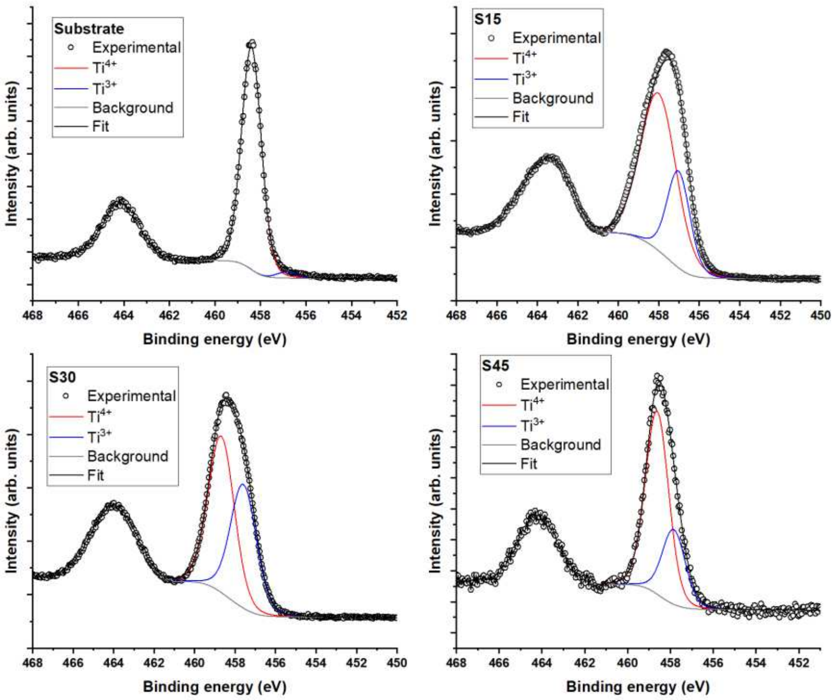

Figure 7: Ti2p high-resolution spectra of the substrate, S15, S30, and S45.

As stated previously, titania is one of the best-known inorganic photocatalysts. By anodizing Ti, we envisioned producing Ti(IV) oxide. Figure 7 reports the Ti2p high-resolution peak of all the samples. For the anodized substrate, the BE of the Ti2p1/2 and Ti2p3/2 states were located at 464.6 and 458.7 eV, respectively, indicative of Ti^{4+} (TiO_2) [2] and confirming the correct synthesis of the TiO_2 NT grown on the titanium felt. After deposition of the Cu_2O phase, a contribution corresponding to Ti^{3+} species appears. Since the sample underwent polarization in the high cathodic regime it is expected that oxygen vacancies arise and some Ti^{3+} species can be formed. Oxygen vacancies and Ti^{3+} species have already been linked to high responsiveness to light with a wavelength between 400 and 800 nm and stable photoactivity in a previous study by acting as traps to prevent the recombination of charge carriers [49]. The calculated ratio Ti^{3+} (457.3 eV)/ Ti^{4+} (458.7 eV) increases with the electrodeposition step. This proves that we reduce Ti^{4+} to Ti^{3+} while electrodepositing Cu_2O, which is logical since it is a reduction step in the synthesis pathway. Furthermore, the electroreduction under 15 minutes (S15) causes an unexpected shape of the Ti2p3/2 peak with a broadening and asymmetry appearing at the higher BE side. In a recent explanatory guide, some of the effects heterostructure characteristics have on XPS spectra and the challenges they present for investigation were emphasized by Chambers et al [50]. Charge buildup at the surface can lead to physical phenomena like built-in potentials and band bending. The variations in potentials brought on by this charge accumulation can change the peaks in binding energy and the geometries of the XPS peaks. In the case of S15, this potential gradient causes photoelectrons to emit with slightly different potentials in each layer, which causes them to emerge at shifted BE and with asymmetrically expanded line morphologies. This could be explained by the fact that this material has a intrinsically different electronic structure compared to that of the substrate.

The Cu2p and CuLMM Auger transitions were also recorded to investigate the oxidation state of the deposited phase. These can be found in the Figures S3 and S4 of the supplementary document. The XPS peaks at 932.7 eV (Cu2p3/2) and 952.7 eV (Cu2p1/2) and the shoulders observed at 932.2 eV are highly consistent with Cu(I) in Cu_2O [51]. There is also an indication of Cu(II) satellite features and a fraction assigned to Cu(II) species at 933.5 eV. This is an unavoidable consequence of doing ex-situ XPS. Concerning the Auger CuLMM transition, a clear peak is present at 570 eV, further confirming that Cu_2O was deposited [8]. The measured X-Ray diffractograms of the plain titania nanotubes before and after different deposition times are shown in Figure S5. Diffractions caused by the titanium felt (highlighted in black) are clearly visible in all three XRDs alongside four diffractions characteristic of anatase TiO_2 (highlighted in blue). After 30 and 45 minutes of deposition, the XRD shows characteristic diffractions for Cu_2O (highlighted in green). These findings further confirm the XPS results. The Cu_2O phase was successfully decorated on the surface of the TNTs.

3.3 Electronic properties study with UPS

A sputter-cleaned Ag sample was used to first calibrate the binding energies obtained with UPS. Figure 8 shows the valence band density of states of the sputter-cleaned Ag sample (intensity vs. binding energy) for both unbiased (black) and biased (blue) conditions. Biasing the sample in UPS is not only useful to overcome the difference in work function between the analyzer and sample, but it is also necessary because, at the cut-off, the electrons have a kinetic energy (KE) of 0 eV and are very sensitive to remaining fields in the analysis chamber. For the Ag reference sample, a WF of 4.35 eV was obtained, in accordance to previously reported values in the range of 4.26-4.74 eV [52].

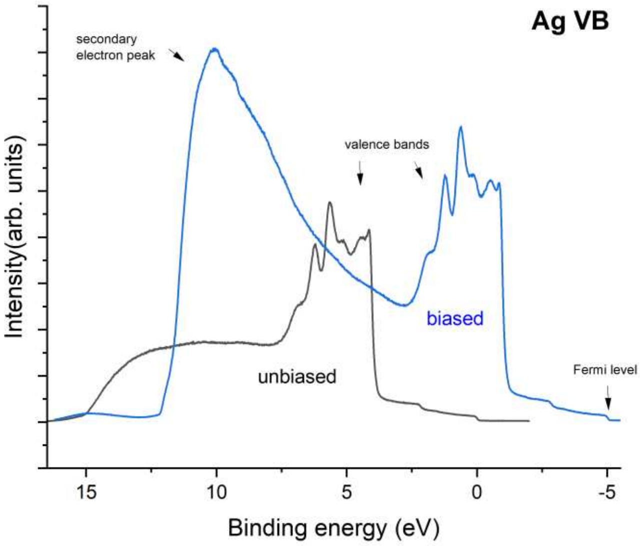

Figure 8: UPS spectra (Intensity vs. binding energy) of a sputter-cleaned Ag reference sample.

Recent research on TiO_2 has shown that some species (organics, water) found in ambient air at low quantities are preferentially adsorb to its surface [53]. This is also confirmed by the recorded C1s spectra, previously reported in Figure 6. Precaution thus needs to be taken when examining UPS results since these vary consequently between a contaminated and clean surface [54]. A GCIB gun with a raster size of 5x5 mm and voltage of 10 kV was used for 30 seconds to this end. This time was enough to remove the carbon contamination. UPS spectra were always preceded and followed by an XPS survey to confirm the correct sample cleaning with the beam. The UPS spectra from the substrate and the three sputter-cleaned Z-schemes were then recorded by applying a bias of -5 V (Figure 9) to better differentiate the electron cut-off. Table 3 reports all the parameters extracted from the spectra for both the substrate and Z-schemes.

The values of E_{cutoff} and E_{VBM} have been recently reported for rutile and anatase titania powders and are in accordance with the values from Table 3 [48]. The WF of the substrate was also recorded to be around an average of 4.29 ± 0.02 eV, corresponding to a literature value of 4.2 eV [9]. With the deposition of the Cu_2O phase, a major decrease in WF and IP is observed, reaching values of 3.67 ± 0.01 and 6.01 ± 0.04 eV, respectively. With increasing deposition times (30 and 45 minutes), these values increase again but remain below the substrate's reported values. This might be explained by the increasing coverage of the Cu_2O particles alongside their increase in size, hindering the proper transfer of electrons. The WF and IP were plotted over the deposition time and shown in Figure 10.

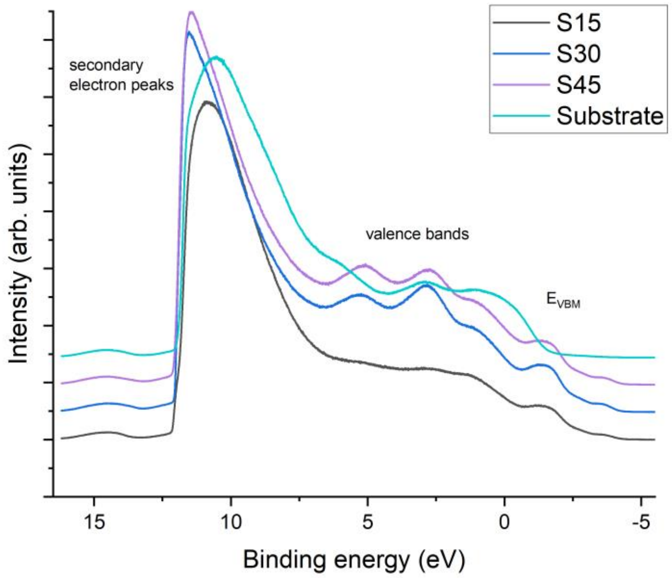

Figure 9: UPS spectra (Intensity vs. binding energy) of the four samples with a -5V bias applied.

Table 3: Electronic parameters extracted with the Multipak Edge tool (eV) and using equations [1] and [2].

Electronic parameters	*substrate*	*15 min*	*30 min*	*45 min*
E_{cutoff}	11.93 ± 0.02	12.55 ± 0.01	12.13 ± 0.01	12.14 ± 0.04
E_{VBM}	-1.64 ± 0.03	-2.66 ± 0.03	-2.59 ± 0.04	-2.57 ± 0.03
Calculated WF	4.29 ± 0.02	3.67 ± 0.01	4.09 ± 0.01	4.08 ± 0.04
Calculated IP	7.65 ± 0.05	6.01 ± 0.04	6.50 ± 0.05	6.52 ± 0.07

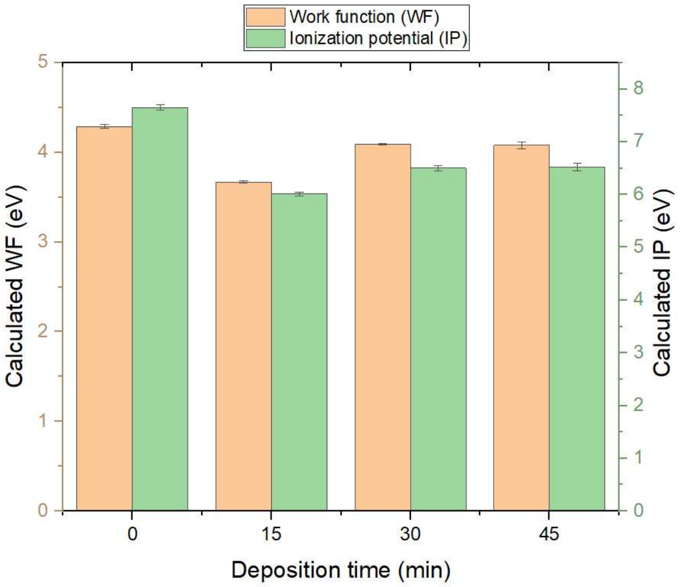

Figure 10: WF and IP plotted over the deposition time of the Cu_2O phase.

The variation of the deposition times of the Cu_2O phase on a TiO_2 NT substrate translates into a modification of the electronic parameters of the $Cu_2O||TiO_2$. Figure 10 and Table 3 reveal that, in comparison to the substrate, the $Cu_2O||TiO_2$ systems present a smaller WF, indicating that they require lower thermodynamic energy to extract an electron from inside the solid to a point in vacuum. This makes it easy to excite electrons, which should lead to improved photocatalytic efficiency when exposed to visible light [55]. The Z-schemes also present a smaller IP, which implies that less work is required to bring the electrons from the VB to E_{vac}. When going to too high values of electrodeposition reduction time, the WF and IP increase again in value, demonstrating that an optimal deposition time, related to specific material features, exists (below 30 minutes). Figure 11 gathers the band diagrams from both the substrate and the 15 minutes electroreduced sample. These are drawn according to vaccum level (0). The incorporation of Cu_2O allows a reduction of the WF and IP values, alongside with a reduction of the bandgap (Eg), beneficial to absorb visible light, which makes up to 43% of the solar radiation reaching the Earth. This further confirms the XPS findings shown in section 3.2 alongside the conclusion that was made for which the sample under 15 minute electroreduction could have fundamentally the most different electronic structure than the substrate.

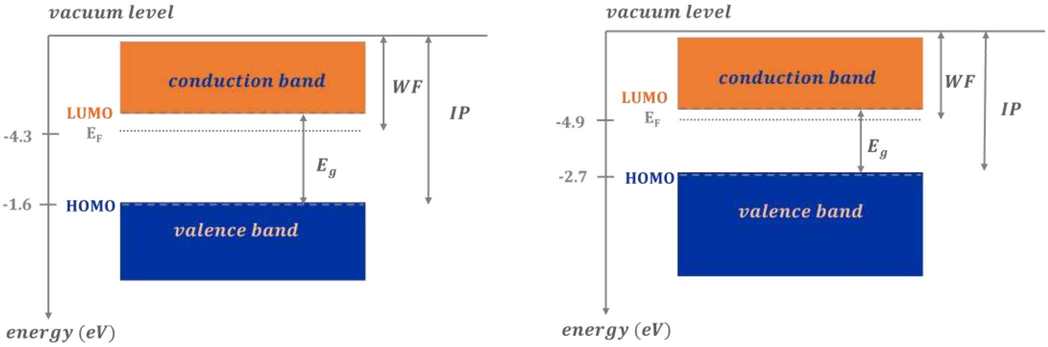

Figure 11: Band diagram of the substrate (left) and of the 15 minutes electroreduced sample (right) with the respective electronic parameters extracted from the UPS spectra.

3.4 Absorption characteristics under visible light

Light absorption profiles of the TiO_2 substrate and $Cu_2O||TiO_2$ Z-schemes were examined. The measured reflectance and transmittance spectra are presented in Figure 12, from which the absorbance can be calculated (Figure 13) as the sum of the reflectance, transmittance, and absorbance at each wavelength equals 100 %. The TiO_2 substrate shows a higher reflectance than the $Cu_2O||TiO_2$ Z-schemes, with the highest difference at 400 nm, while less spectral variation is present in the transmittance spectra. Considering the $Cu_2O||TiO_2$ Z-schemes, increasing reflectance and decreasing transmittance can be observed with increasing deposition times, giving rise to a decreasing absorbance with deposition time. For both the substrate and $Cu_2O||TiO_2$ Z-schemes, high absorbance values exceeding 87 % are observed. The addition of the narrow bandgap semiconductor Cu_2O on the TiO_2 nanotube arrays creates extra absorption between 400 and 600nm and slightly decreases it from 600 nm.

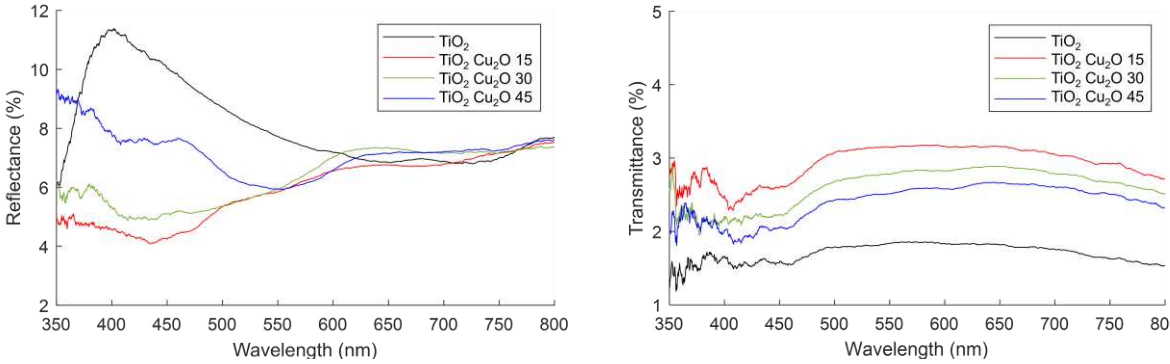

Figure 12: Reflectance (left) and transmittance (right) spectra for the substrate and Z-schemes.

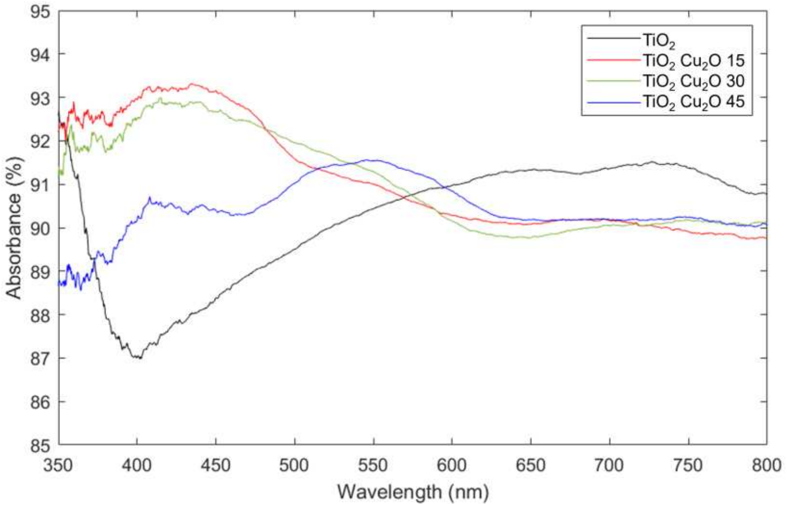

Figure 13: Absorbance spectra from the substrate and the Z-scheme materials, calculated using MATLAB.

It is also observed that the bare titania presents a broad absorption in the visible range namely from 400-600 nm. This is related to its electronic structure, and because a number of vibrational energy levels are available at each electronic energy level. An important factor enhancing the visible light absorption of titania is related to the increase in surface area and porosity of nanostructured titania, namely the growth of ordered nanotubes via the method employed in this work.

Table 4: Integrals for each of the absorbance spectra calculated from 350 nm to 800nm.

Sample reference	Substrate	S15	S30	S45
A_{Samp}-A_{Subs}	0	430	393	106

The integrals for each of the absorbance spectra were calculated from 350 to 800 nm and are shown in **Fout! Verwijzingsbron niet gevonden.**. There is an optimal deposition time (15 minutes) for which the area under the absorbance curve reaches a maximum. The same trend as the one reported in paragraph 3.3 is observed: the $Cu_2O||TiO_2$ systems present higher absorbance in the visible light range than the substrate, with a maximum reached at the shortest deposition time used (15 minutes), a condition for which the WF and IP are at their lowest value. The UPS data are thus in good agreement with the empirical absorption profiles of $Cu_2O||TiO_2$.

Conclusions

Cu_2O-modified TiO_2 photocatalysts with different Cu_2O deposition times were prepared via anodization and electrochemical deposition with the intention of creating a Z-scheme semiconductor with better visible light absorption efficiency. Very surface-sensitive UPS provided meaningful quantitative and qualitative insights about the electronic parameters of the TiO_2 substrate and of the differently synthesized samples, such as Fermi level position, electron cut-off, valence band maximum, work function, and ionization potential. The UPS results revealed that all the $TiO_2||Cu_2O$ Z-schemes present a lower work function with respect to the TiO_2 substrate, meaning that the electrons close to the conduction band are more easily photoexcited and released in vacuum. A lower ionization potential was also observed for the Z-schemes with respect to the substrate, implying less work is required to bring the electrons from the VB to E_{vac}, convenient to facilitate the excitation of electrons. These materials are thus expected to achieve better performance under visible light conditions.

Complimentary FE-SEM, EDX and XPS provided insights in the morphology, composition and chemical bonding and oxidation states of the samples surface. Parameters such as particle size and surface coverage were controlled via the variation of an important synthetic parameter: the deposition time of the Cu_2O phase. The variation of this parameter had an impact in the electronic properties of the systems. The shortest considered electrodeposition times (15 minutes) yielded the most convenient material in terms of morphology and electronic properties, without the TiO_2 nanotubes at the surface being mostly covered with Cu_2O nanoparticles and with the lowest WF and IP, making it optimal for the transport of photogenerated carriers. The visible light absorption performance of $Cu_2O||TiO_2$ under different electrodeposition times correlated with the reported UPS results. The Z-schemes with the shortest deposition time under the conditions of this study and thus lowest WF and IP presented the highest absorption in the visible light range.

In essence, this work proposes a valuable methodology for band diagram tracing from UPS spectra and provides new insights in the relationship between synthesis, electronic properties and visible light absorption of titania based Z-schemes for photocatalytic applications with a combination of surface sensitive techniques and optical absorption studies.

Future work includes testing the performance of the catalysts in a built-in reactor as well as probing the conduction band states of the samples and obtaining a full description of their electronic structure using complementary techniques such as spectrochemical analysis or Low-Energy Inverse Photoemission Spectroscopy (LEIPS), which extracts the electron affinities of solid samples within 0.1 eV of accuracy.

Acknowledgments

The authors would like to acknowledge the VLAIO Moonshot SYNCAT project (HBC.2020.2614) launched by the Flemish government in the framework of the 'Flanders Industry Innovation Moonshot' initiative. The authors would also like to thank J. Mann and K. Artyushkova from ULVAC-PHI and K. Baert from Vrije Universiteit Brussel for their insightful comments and help with the PHI VersaProbe III equipment.

CRediT authorship contribution statement

Beatriz de la Fuente: Conceptualization, Investigation, Methodology, Visualization, Writing - original draft. **Jan Bomnuter**: Investigation, Methodology, Visualization, Writing - original draft. **Michele del Moro**: Investigation, Methodology, Visualization, Writing - original draft. **Lien Smeesters**: Investigation, Methodology, Visualization, Writing - original draft. **Vanina Cristaudo**: Validation, Writing - review & editing. **Tom Bruegelmans**: Funding acquisition, Project administration, Supervision. **Vera Meynen**: Methodology, Supervision, Validation, Writing - review & editing. **Pegie Cool**: Supervision, Validation, Writing - review & editing. **Annick Hubin**: Methodology, Supervision, Validation, Writing - review & editing. **Tom Hauffman**: Funding acquisition, Methodology, Project administration, Supervision, Validation, Writing - review & editing.

Funding

This work was supported by Moonshot Flanders Industry Innovation (cSBO in MOT3 Electrification & Radical Process Transformation) and by the Research Foundation Flanders (FWO) for XPS infrastructure funding (I006220N).

References

[1] S. Chu and A. Majumdar, "Opportunities and challenges for a sustainable energy future," *Nature*, vol. 488, no. 7411. pp. 294–303, Aug. 16, 2012. doi: 10.1038/nature11475.

[2] N. S. Lewis and D. G. Nocera, "Powering the planet: Chemical challenges in solar energy utilization," 2006. [Online]. Available: www.pnas.orgcgidoi10.1073pnas.0603395103

[3] B. Kumar, M. Llorente, J. Froehlich, T. Dang, A. Sathrum, and C. P. Kubiak, "Photochemical and photoelectrochemical reduction of CO2," *Annual Review of Physical Chemistry*, vol. 63. Annual Reviews Inc., pp. 541–569, 2012. doi: 10.1146/annurev-physchem-032511-143759.

[4] A. Machín, M. Cotto, J. Ducongé, and F. Márquez, "Artificial Photosynthesis: Current Advancements and Future Prospects," *Biomimetics*, vol. 8, no. 3, p. 298, Jul. 2023, doi: 10.3390/biomimetics8030298.

[5] D. Gust, T. A. Moore, and A. L. Moore, "Solar fuels via artificial photosynthesis," *Acc Chem Res*, vol. 42, no. 12, pp. 1890–1898, Dec. 2009, doi: 10.1021/ar900209b.

[6] Inoue T, Fujishima A, and Konishi S, "Photoelectrocatalytic reduction of carbon dioxide in aqueous suspensions of semiconductor powders," *Nature*, vol. 277, pp. 637–638, 1979.

[7] X. Shao *et al.*, "Metal chalcogenide-associated catalysts enabling CO2electroreduction to produce low-carbon fuels for energy storage and emission reduction: catalyst structure, morphology, performance, and mechanism," *Journal of Materials Chemistry A*, vol. 9, no. 5. Royal Society of Chemistry, pp. 2526–2559, Feb. 07, 2021. doi: 10.1039/d0ta09232k.

[8] J. Cai, J. Huang, M. Ge, and Y. Lai, "Multidimensional TiO2 nanostructured catalysts for sustainable H2 generation," in *Multifunctional Photocatalytic Materials for Energy*, Elsevier Inc., 2018, pp. 237–288. doi: 10.1016/B978-0-08-101977-1.00012-0.

[9] H. Park, H. il Kim, G. H. Moon, and W. Choi, "Photoinduced charge transfer processes in solar photocatalysis based on modified TiO2," *Energy Environ Sci*, vol. 9, no. 2, pp. 411–433, Feb. 2016, doi: 10.1039/c5ee02575c.

[10] R. Li, T. Li, and Q. Zhou, "Impact of titanium dioxide (TiO2) modification on its application to pollution treatment—a review," *Catalysts*, vol. 10, no. 7. MDPI, Jul. 01, 2020. doi: 10.3390/catal10070804.

[11] M. Mishra and D. M. Chun, "α-Fe2O3 as a photocatalytic material: A review," *Applied Catalysis A: General*, vol. 498. Elsevier B.V., pp. 126–141, Jun. 05, 2015. doi: 10.1016/j.apcata.2015.03.023.

[12] D. Zhang, "Synergetic effects of Cu2O photocatalyst with titania and enhanced photoactivity under visible irradiation," *Acta Chimica Slovaca*, vol. 6, no. 1, pp. 141–149, May 2013, doi: 10.2478/acs-2013-0022.

[13] C. Xu *et al.*, “Preparation of ZnO/Cu2O compound photocatalyst and application in treating organic dyes,” *J Hazard Mater*, vol. 176, no. 1–3, pp. 807–813, Apr. 2010, doi: 10.1016/j.jhazmat.2009.11.106.

[14] A. Malathi, J. Madhavan, M. Ashokkumar, and P. Arunachalam, “A review on BiVO4 photocatalyst: Activity enhancement methods for solar photocatalytic applications,” *Applied Catalysis A: General*, vol. 555. Elsevier B.V., pp. 47–74, Apr. 05, 2018. doi: 10.1016/j.apcata.2018.02.010.

[15] F. Wang, C. DiValentin, and G. Pacchioni, “Rational Band Gap Engineering of WO 3 Photocatalyst for Visible light Water Splitting,” *ChemCatChem*, vol. 4, no. 4, pp. 476–478, Apr. 2012, doi: 10.1002/cctc.201100446.

[16] I. M. Szilágyi *et al.*, “WO 3 photocatalysts: Influence of structure and composition,” *J Catal*, vol. 294, pp. 119–127, Oct. 2012, doi: 10.1016/j.jcat.2012.07.013.

[17] Q. Xu, L. Zhang, J. Yu, S. Wageh, A. A. Al-Ghamdi, and M. Jaroniec, “Direct Z-scheme photocatalysts: Principles, synthesis, and applications,” *Materials Today*, vol. 21, no. 10. Elsevier B.V., pp. 1042–1063, Dec. 01, 2018. doi: 10.1016/j.mattod.2018.04.008.

[18] J. Low, C. Jiang, B. Cheng, S. Wageh, A. A. Al-Ghamdi, and J. Yu, “A Review of Direct Z-Scheme Photocatalysts,” *Small Methods*, vol. 1, no. 5. John Wiley and Sons Inc, May 01, 2017. doi: 10.1002/smtd.201700080.

[19] W. Yu, D. Xu, and T. Peng, “Enhanced photocatalytic activity of g-C3N4 for selective CO2 reduction to CH3OH via facile coupling of ZnO: A direct Z-scheme mechanism,” *J Mater Chem A Mater*, vol. 3, no. 39, pp. 19936–19947, Aug. 2015, doi: 10.1039/c5ta05503b.

[20] P. Zhou, J. Yu, and M. Jaroniec, “All-solid-state Z-scheme photocatalytic systems,” *Advanced Materials*, vol. 26, no. 29. Wiley-VCH Verlag, pp. 4920–4935, Aug. 06, 2014. doi: 10.1002/adma.201400288.

[21] K. Nakata and A. Fujishima, “TiO 2 photocatalysis: Design and applications,” *Journal of Photochemistry and Photobiology C: Photochemistry Reviews*, vol. 13, no. 3. pp. 169–189, Sep. 2012. doi: 10.1016/j.jphotochemrev.2012.06.001.

[22] Y. Wang, M. Zu, X. Zhou, H. Lin, F. Peng, and S. Zhang, “Designing efficient TiO2-based photoelectrocatalysis systems for chemical engineering and sensing,” *Chemical Engineering Journal*, vol. 381. Elsevier B.V., Feb. 01, 2020. doi: 10.1016/j.cej.2019.122605.

[23] R. Song *et al.*, “Highly Efficient Degradation of Persistent Pollutants with 3D Nanocone TiO2-Based Photoelectrocatalysis,” *J Am Chem Soc*, vol. 143, no. 34, pp. 13664–13674, Sep. 2021, doi: 10.1021/jacs.1c05008.

[24] L. Kavan, “Conduction band engineering in semiconducting oxides (TiO2, SnO2): Applications in perovskite photovoltaics and beyond,” *Catalysis Today*, vol. 328. Elsevier B.V., pp. 50–56, May 15, 2019. doi: 10.1016/j.cattod.2018.10.065.

[25] A. J. Frank, N. Kopidakis, and J. Van De Lagemaat, “Electrons in nanostructured TiO2 solar cells: Transport, recombination and photovoltaic properties,” *Coordination Chemistry Reviews*, vol. 248, no. 13–14. pp. 1165–1179, Jul. 2004. doi: 10.1016/j.ccr.2004.03.015.

[26] J. M. Macak, M. Zlamal, J. Krysa, and P. Schmuki, “Self-organized TiO2 nanotube layers as highly efficient photocatalysts,” *Small*, vol. 3, no. 2, pp. 300–304, Feb. 2007, doi: 10.1002/smll.200600426.

[27] H. Dong *et al.*, “An overview on limitations of TiO2-based particles for photocatalytic degradation of organic pollutants and the corresponding countermeasures,” *Water Research*, vol. 79. Elsevier Ltd, pp. 128–146, Aug. 01, 2015. doi: 10.1016/j.watres.2015.04.038.

[28] D. Gong *et al.*, “RAPID COMMUNICATIONS Titanium oxide nanotube arrays prepared by anodic oxidation,” 2001.

[29] C. A. Grimes, “Synthesis and application of highly ordered arrays of TiO2 nanotubes,” *J Mater Chem*, vol. 17, no. 15, pp. 1451–1457, 2007, doi: 10.1039/b701168g.

[30] M. E. Aguirre, R. Zhou, A. J. Eugene, M. I. Guzman, and M. A. Grela, “Cu2O/TiO2 heterostructures for CO2 reduction through a direct Z-scheme: Protecting Cu2O from photocorrosion,” *Appl Catal B*, vol. 217, pp. 485–493, 2017, doi: 10.1016/j.apcatb.2017.05.058.

[31] T. Schultz *et al.*, “Reliable Work Function Determination of Multicomponent Surfaces and Interfaces: The Role of Electrostatic Potentials in Ultraviolet Photoelectron Spectroscopy,” *Adv Mater Interfaces*, vol. 4, no. 19, Oct. 2017, doi: 10.1002/admi.201700324.

[32] S. Kashiwaya, J. Morasch, V. Streibel, T. Toupance, W. Jaegermann, and A. Klein, “The Work Function of TiO2,” *Surfaces*, vol. 1, no. 1, pp. 73–89, Sep. 2018, doi: 10.3390/surfaces1010007.

[33] A. Kahn, “Fermi level, work function and vacuum level,” *Materials Horizons*, vol. 3, no. 1. Royal Society of Chemistry, pp. 7–10, Jan. 01, 2016. doi: 10.1039/c5mh00160a.

[34] S. Yamamoto, “Fundamental physics of vacuum electron sources,” *Reports on Progress in Physics*, vol. 69, no. 1, pp. 181–232, Jan. 2006, doi: 10.1088/0034-4885/69/1/R04.

[35] R. W. Strayer, W. Mackie, and L. W. Swanson, “WORK FUNCTION MEASUREMENTS BY THE FIELD EMISSION RETARDING POTENTIAL METHOD*.”

[36] J. S. Kim *et al.*, “Synthetic Metals 111-112,” 2000. [Online]. Available: www.elsevier.comrlocatersynmet

[37] J. W. Kim and A. Kim, “Absolute work function measurement by using photoelectron spectroscopy,” *Current Applied Physics*, vol. 31. 2021. doi: 10.1016/j.cap.2021.07.018.

[38] W. C. Price, “PHOTOELECTRON SPECTROSCOPY A. Introductory Survey.”

[39] R. Schlaf, H. Murata, and Z. H. Kafafi, “Work function measurements on indium tin oxide films,” 2001. [Online]. Available:

www.elsevier.nl/locate/elspecRapidcommunication

[40] Y. Liao *et al.*, "A Facile Method for Preparation of Cu2O-TiO2 NTA Heterojunction with Visible-Photocatalytic Activity," *Nanoscale Res Lett*, vol. 13, 2018, doi: 10.1186/s11671-018-2637-8.

[41] Y. Li, W. Zhang, X. Shen, P. Peng, L. Xiong, and Y. Yu, "Octahedral Cu2O-modified TiO2 nanotube arrays for efficient photocatalytic reduction of CO2," *Cuihua Xuebao/Chinese Journal of Catalysis*, vol. 36, no. 12, pp. 2229–2236, Dec. 2015, doi: 10.1016/S1872-2067(15)60991-3.

[42] I. Robel, M. Kuno, and P. v. Kamat, "Size-dependent electron injection from excited CdSe quantum dots into TiO2 nanoparticles," *J Am Chem Soc*, vol. 129, no. 14, pp. 4136–4137, Apr. 2007, doi: 10.1021/ja070099a.

[43] D. R. Baker and P. v. Kamat, "Photosensitization of TiO2 nanostructures with CdS quantum dots: Particulate versus tubular support architectures," *Adv Funct Mater*, vol. 19, no. 5, pp. 805–811, Mar. 2009, doi: 10.1002/adfm.200801173.

[44] J. M. Macak, B. G. Gong, M. Hueppe, and P. Schmuki, "Filling of TiO2 nanotubes by self-doping and electrodeposition," *Advanced Materials*, vol. 19, no. 19, pp. 3027–3031, Oct. 2007, doi: 10.1002/adma.200602549.

[45] M. R. Alexander, G. Beamson, P. Bailey, T. C. Q. Noakes, P. Skeldon, and G. E. Thompson, "The distribution of hydroxyl ions at the surface of anodic alumina," *Surface and Interface Analysis*, vol. 35, no. 8, pp. 649–657, Aug. 2003, doi: 10.1002/sia.1585.

[46] M. C. Biesinger, "Accessing the robustness of adventitious carbon for charge referencing (correction) purposes in XPS analysis: Insights from a multi-user facility data review," *Appl Surf Sci*, vol. 597, Sep. 2022, doi: 10.1016/j.apsusc.2022.153681.

[47] J. Han *et al.*, "Mechanistic investigation on tuning the conductivity type of cuprous oxide (Cu2O) thin films via deposition potential," *Int J Hydrogen Energy*, vol. 43, no. 30, pp. 13764–13777, Jul. 2018, doi: 10.1016/j.ijhydene.2018.02.121.

[48] M. C. Biesinger, L. W. M. Lau, A. R. Gerson, and R. S. C. Smart, "Resolving surface chemical states in XPS analysis of first row transition metals, oxides and hydroxides: Sc, Ti, V, Cu and Zn," *Appl Surf Sci*, vol. 257, no. 3, pp. 887–898, Nov. 2010, doi: 10.1016/j.apsusc.2010.07.086.

[49] X. Bi *et al.*, "Tuning oxygen vacancy content in TiO2 nanoparticles to enhance the photocatalytic performance," *Chem Eng Sci*, vol. 234, Apr. 2021, doi: 10.1016/j.ces.2021.116440.

[50] S. A. Chambers, L. Wang, and D. R. Baer, "Introductory guide to the application of XPS to epitaxial films and heterostructures," *Journal of Vacuum Science & Technology A*, vol. 38, no. 6, p. 061201, Dec. 2020, doi: 10.1116/6.0000465.

[51] F. Bi, M. F. Ehsan, W. Liu, and T. He, "Visible-light photocatalytic conversion of carbon dioxide into methane using Cu2O/TiO2 hollow nanospheres," *Chin J Chem*, vol. 33, no. 1, pp. 112–118, 2015, doi: 10.1002/cjoc.201400476.

[52] W. M. Haynes, "CRC Handbook of Chemistry and Physics 95th Edition."

[53] J. Balajka *et al.*, "High-affinity adsorption leads to molecularly ordered interfaces on TiO2 in air and solution," *Science (1979)*, vol. 361, no. 6404, pp. 786–789, Aug. 2018, doi: 10.1126/science.aat6752.

[54] A. Klein, "Transparent conducting oxides: Electronic structure-property relationship from photoelectron spectroscopy with in situ sample preparation," *Journal of the American Ceramic Society*, vol. 96, no. 2, 2013, doi: 10.1111/jace.12143.

[55] Charles Kittel, *Introduction to Solid State Physics*. 2005.